Catalytic methane pyrolysis in molten $MnCl_2$-KCl

Dohyung Kang[a], Nazanin Rahimi[a], Michael J. Gordon[a], Horia Metiu[b], Eric W. McFarland[a,*]

[a] Department of Chemical Engineering, University of California, Santa Barbara, CA, 93106-5080, USA
[b] Department of Chemistry and Biochemistry, University of California, Santa Barbara, CA, 93106-9510, USA

ARTICLE INFO

ABSTRACT

Methane decomposition to produce molecular hydrogen and solid carbon was catalyzed by contact with molten $KCl:MnCl_2$ mixtures in a bubble column reactor from 700 to 1050 °C. The apparent activation energy decreased from approximately 300 kJ/mole for pure KCl to 161 kJ/mole in a 67:33 mol % mixture of $KCl:MnCl_2$. At 30% methane conversion, pyrolysis in the $KCl:MnCl_2$ melt at 1050 °C had high hydrogen selectivity (~99%) in comparison to pure molten KCl (~90%), which was observed to produce multiple hydrocarbon co-products. The pyrolysis activity of the $KCl:MnCl_2$ melt remained stable for over 30 h and produced a separable, highly graphitic carbon solid that accumulated at the surface of the higher-density salt melt.

1. Introduction

Hydrogen is an essential chemical feedstock used in the synthesis of chemicals critical to the global economy. Many studies have examined the possibility that hydrogen, which burns without producing CO_2, might be a preferred fuel for the future [1–3]. Today the most economical process for producing hydrogen commercially is by reforming and processing methane with steam ($CH_4 + 2H_2O \rightarrow CO_2 + 4H_2$). This process produces approximately 50 million tons of H_2 per year and 300 million tons of CO_2 as an unwanted co-product. Although sequestration of carbon dioxide in the earth has been demonstrated, there is no evidence that it can be deployed commercially at a competitive cost. Thus steam methane reforming for hydrogen production is not suitable to achieve significant carbon dioxide emissions reductions and create an economically sustainable hydrogen-based energy infrastructure.

Nevertheless, methane will likely be abundant and widely available at low-cost for several decades due to the decreasing costs of producing natural gas from unconventional reservoirs such as shale gas [4]. Use of this resource in processes that produce H_2 but do not emit CO_2 would provide a near-term economical energy resource and allow H_2 infrastructure deployment at significant scales to prepare society for a future when low-cost fossil resources become scarce (and thus more costly) and H_2 might be produced more sustainably from water using nuclear power or other sources.

One alternative to reforming with steam is methane pyrolysis, $CH_4 \rightarrow C + 2H_2$, which produces no carbon dioxide; instead, a solid carbon product is made which is more readily separated, transported and stored. Gas-phase, non-catalytic, CH_4 pyrolysis requires elevated

operating temperature (> 1200 °C), and has low selectivity to hydrogen [5–8]; it is not presently economical. To develop a cost competitive hydrogen production process by methane pyrolysis one needs to find a catalyst and create a reaction environment from which the solid carbon can be economically removed. Solid transition metals, which are good catalysts, have been widely studied [9–12], but they are deactivated by coking. The catalyst can be reactivated by gasification of the carbon with O_2 [13], H_2O [14], or CO_2 [15], however, these procedures give rise to undesirable CO_2 emissions. Coke removal by an acid treatment [16] is prohibitively expensive.

One approach for avoiding deactivation by coke is to contact the methane with a liquid catalyst where the catalyst surface is continuously renewed. In a bubble column reactor, each methane containing bubble will contact a carbon-free melt surface. As the bubble rises through the molten bed, the methane is pyrolyzed and forms solid carbon on the walls of the bubble. The carbon rises with the bubble and ends up at the surface of the melt. Thus, the bulk of the molten metal is carbon free and each methane bubble is in contact with an uncontaminated surface. Because methane pyrolysis takes place at high temperature the only usable liquids are molten metals [17–24] or certain molten salts.

Molten salts have been previously used as a medium for pyrolysis of hydrocarbon containing materials, including propane, aromatic compounds [25,26], and biomass [27]. The solid carbon produced in the molten salt systems can potentially be separated as a value-added product [28,29]. Any residual salts in the carbon products are often highly soluble in water, facilitating purification of the carbon. Chemical activation and pyrolysis of CH_4 is more difficult than other

---

* Corresponding author.
E-mail address: ewmcfar@engineering.ucsb.edu (E.W. McFarland).

hydrocarbons and there are few studies on CH_4 pyrolysis in molten salt media.

We describe results from pyrolysis of CH_4 catalyzed by a molten mixture of manganese chloride ($MnCl_2$) and potassium chloride (KCl). Manganese is an abundant element that has been studied as an active site for C–H bond activation [30]. Kenney's review of molten salt catalysis [25] mentions that molten $MnCl_2$ readily pyrolyzes propane. We have explored the use of molten mixtures of $MnCl_2$ with KCl for methane pyrolysis. While KCl is a poor catalyst and $MnCl_2$ is a mediocre one, a mixture of 67:33 KCl with $MnCl_2$ is the best molten salt catalyst for methane pyrolysis discovered so far. We specifically address the following questions related to CH_4 pyrolysis in molten $MnCl_2$-KCl: (1) What is the temperature dependent activity in molten $MnCl_2$ and in $MnCl_2$-KCl salt mixtures?, (2) Is the salt activity stable during sustained operation?, (3) Is the solid carbon produced separable from the salt mixture?, (4) What are the structural characteristics of the solid carbon products? and, (5) What are the reaction mechanisms for CH_4 pyrolysis in $MnCl_2$-KCl molten salt mixtures?

2. Experimental

2.1. Preparation of molten $MnCl_2$-KCl

Several mixtures of anhydrous $MnCl_2$ (Sigma Aldrich, ≥98%) and KCl (Sigma Aldrich, ≥99%) were prepared as $MnCl_2(x)$-$KCl(100-x)$, with mole percentages, x, of 0, 17, 33. 50, 67, and 100. The mixture of solid salts was further dehydrated under vacuum, at 200 °C, for more than 12 h, and then melted in a quartz reactor. The melting temperatures of these mixtures are approximately 770 °C, 650 °C, 410 °C, 490 °C, 500 °C, and 650°C, respectively [31]. Dry HCl was bubbled through the salt during melting to suppress hydration. The melt mixtures were prepared in an oxygen-free environment and melted within the quartz reactor tubes prior to the pyrolysis experiments.

2.2. Bubble column experiments

The bubble column was mounted inside a temperature-controlled, electrically heated furnace such that 12.5 cm of molten salt and 12.5 cm of headspace (for disengagement) were in the hot zone (Fig. 1). To suppress gas phase pyrolysis above the bubble column, the reactor headspace above the melt surface was continuously purged with Ar sweep gas (50 sccm). For pyrolysis, the reactant gas was bubbled through a small diameter quartz tube (internal diameter = 0.2 cm) that was inserted from the top; the tube outlet was 1 cm above the bottom of the reactor. The bubble rise distance was 11.5 cm, giving a bubble rise
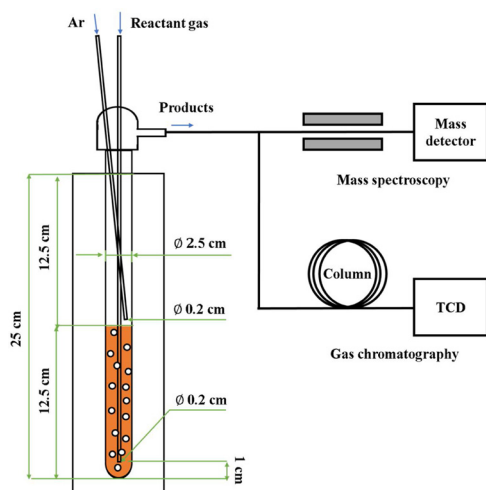

Fig. 1. Schematic diagram of bubble column reactor system.

time ˜0.6 s. The pressure in the inlet tube was monitored to avoid any potential safety hazards caused by clogging of the reactor inlet tube. The reactants and major gas phase effluents were periodically sampled and analyzed by gas chromatography (HP 5890 Series II) using a Molesieve 5A column and thermal conductivity detector. An on-line, differentially pumped mass spectrometer (SRS RGA 200) was used to monitor the products, and detect minor by-products such as C_2 hydrocarbons and aromatics. Mass spectrometer sensitivity factors and pumping factors for the various products were calibrated using gas mixtures of known composition and concentrations.

2.3. Recovery and processing of solid carbon product

The carbon produced by CH_4 pyrolysis was recovered from the bubble column after cooling. The collected solid was transferred to a beaker and the salt residue dissolved into hot deionized water (80 °C). The solid was filtered, rinsed, and rewashed 10 times. The final suspension was filtered and dried overnight at 100 °C.

2.4. Characterization of carbon product

X-ray diffraction was used to characterize the crystalline structure of the carbon product using a Panalytical Empyrean powder diffractometer with a monochromatic Cu-Kα source (λ = 1.54056 Å). The diffraction pattern was collected for 2θ = 10-90° with a step size of 0.013°. Raman spectra were obtained using a Horiba Jobin Yvon LabRAM Aramis equipped with a 633-nm laser. Electron microscopy was performed using an FEI XL30 Sirion FEG SEM operated at 5 keV with an attached energy dispersive X-ray spectrometer (EDX) operated at 20 keV for elemental mapping of the carbon. High-resolution TEM images of the carbon were obtained with an FEI Titan FEG TEM/STEM. The bulk composition and contaminants in the carbon product were measured by X-ray fluorescence (XRF), WDXRF Rigaku ZSX Primus IV. Before XRF, the carbon was pelletized with boric acid.

3. Results and discussion

3.1. Molten salt activity for methane pyrolysis

The conversion of CH_4 in different molten $MnCl_2$-KCl mixtures as a function of temperature is shown in Fig. 2a. The activity of pure KCl is significantly lower than that of any $MnCl_2$-KCl mixture. The conversion increases with the concentration of $MnCl_2$ but pure $MnCl_2$ is less active than $MnCl_2(67)$-$KCl(33)$ (the numbers in parentheses indicate the composition in molar percentages). The fact that pure $MnCl_2$ is less active than $MnCl_2(67)$-$KCl(33)$ indicates that while $MnCl_2$ is the "active component", KCl is not an "inert solvent" but it affects the activity of $MnCl_2$. Fig. 2b shows Arrhenius plots of the rate of methane conversion obtained in a differential reactor (conversion less than 10%). For various reasons, to be discussed shortly, the conversion changes in time; this rate data was taken at early times, and each rate measurement used fresh salt.

The apparent activation energy, determined from the Arrhenius plots, depends upon the composition of the melt as shown in Fig. 2c. The activation energy for pyrolysis in KCl is relatively high. Addition of $MnCl_2$ to monovalent KCl is associated with a reduction in the apparent activation energy. The activation energy decreases substantially for salts having more than 17% $MnCl_2$. It reaches a minimum for $MnCl_2(50)$-$KCl(50)$ and then increases as more $MnCl_2$ is added. The apparent activation energy of molten $MnCl_2$-KCl mixture is compared with previously reported molten and solid catalysts in Table 1. The activation energy of the molten $MnCl_2$-KCl mixture is the lowest among reported molten catalysts and even lower than solid carbon catalysts. There is however a compensation: the pre-exponential increases when the activation energy increases and this is why the rate constant (and therefore the overall reaction rate, moles/m³-s) changes less with
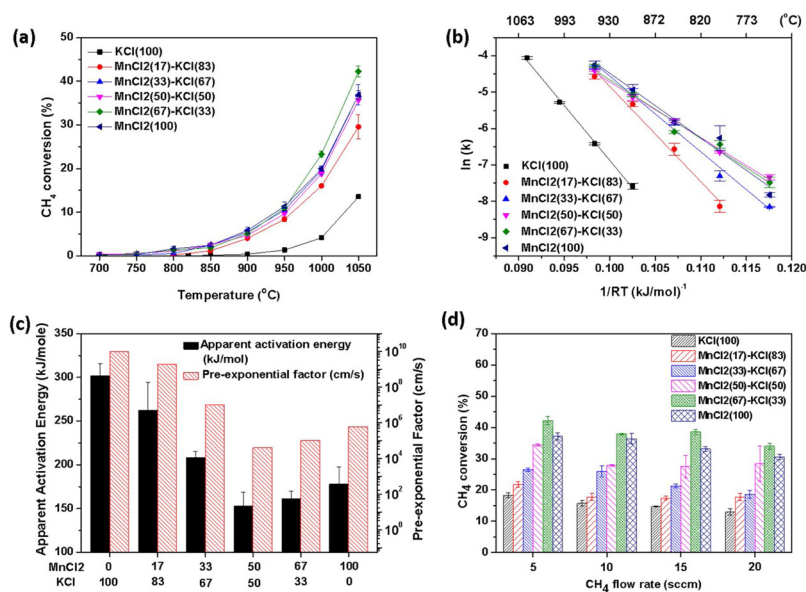
Fig. 2. Activity of molten $MnCl_2$-KCl for CH_4 pyrolysis. (a) CH_4 conversion versus temperature for a $MnCl_2$-KCl bubble column. Melt height 12.5 cm, reactant gas = 20 sccm (50 mol% of CH_4 and 50 mol% of Ar), sweep gas = 50 sccm (100 mol% of Ar). (b) Arrhenius plot for apparent activation energies for methane consumption rate, catalyzed by $MnCl_2$-KCls. (c) Comparison of apparent activation energies and pre-exponential factors of the molten $MnCl_2$-KCl mixtures. (d) CH_4 conversion versus CH_4 flow rate for a 12.5-cm molten $MnCl_2$-KCl bubble column at 1050 °C: reactant gas (100 mol% of CH_4), sweep gas = 50 sccm (100 mol% of Ar).

Table 1
Apparent activation energies of molten salts, metals and solid catalysts.

Catalyst	Apparent activity energy (kJ/mole)	Carbon product
Molten $MnCl_2$(50)-KCl(50)	153 ± 16	Separable
Molten $MnCl_2$(67)-KCl(33)	161 ± 9	Separable
Molten Ni(27)-Bi(73) [23]	208	Separable
Molten Bi [23]	310	Separable
Gas phase [39]	422	Separable
Solid Ni [40]	65	Non-separable
Solid Ni/SiO_2 [41]	96.1	Non-separable
Activated carbon [40]	194	Non-separable
Carbon black [42]	205-264	Non-separable

concentration than the activation energies might suggest. In comparison to the pure KCl with an apparent activation energy of ~300 kJ/mole, the reaction rate in $MnCl_2$(50)-KCl(50) is only approximately 10 times faster despite a factor of two reduction in apparent activation energy. Interpretation of the decreased pre-exponential is difficult without a detailed model, however, one possible explanation is the relatively low surface area of the liquid resulting in a far lower collision rate with the more active salt surface (or vapor phase salt) compared to the total collision rate in the gas phase.

It was previously reported that a molten $MnCl_2$-KCl mixture, contains two predominant molecular ions, $MnCl_4^{2-}$ and $MnCl_6^{4-}$, and their relative ratios in the melt changes with composition [32–37]. For $MnCl_2$ molar fractions greater than 0.67, the concentration of $MnCl_4^{2-}$ decreases and so does the activity of the melt [33]. Excess molar volume and conductivity also showed the singular point at 67:33 mol % mixture of KCl:$MnCl_2$ [32]. One is tempted to suggest that $MnCl_4^{2-}$ is more active catalytically than $MnCl_6^{4-}$. However, CH_4 is not highly soluble in the melt and catalysis is controlled by the surface concentration, which is not known.

$MnCl_2$ has a high vapor pressure (0.13 atm at 1000 °C) which is comparable to the partial pressure of the methane at the inlet (0.5 atm). It is difficult to determine whether the $MnCl_2$ vapor is important or not. When the bubble first enters the reactor, it contains no $MnCl_2$ vapor and it has the maximum methane partial pressure. When the bubble exits the melt, it has much less CH_4 and some accumulated vapor produced by evaporation. Since we don't know the evaporation rate, it is difficult to estimate the concentration of methane and of $MnCl_2$ in the bubble, as the bubble travels through the melt. In addition, there is vapor in the space above the melt, even though this is purged with Ar. With the data

available to us, we cannot determine whether the $MnCl_2$ vapor is an active gas phase catalyst or not. Given the high vapor pressure of $MnCl_2$ and the relatively small pre-exponential for the most active mixtures it is likely reactions on the melt surface are the most important.

Fig. 2d shows the dependence of methane conversion on the flow rate at 1050 °C. The flow rate determines the time in which the bubble grows at the mouth of the tube through which the reactants are introduced. Once the bubble detaches from the tube its rise time through the melt depends on the depth, the bubble size, the melt density and its viscosity. The bubble size and rise velocity are not a strong function of the flowrates [38]. The flow rates are such that the bubbles do not coalesce as they rise through the column. To a first approximation, increasing the flow rate shortens the time the bubble grows at the mouth of the inlet tube (and reacts). As expected, at the slower flow rates, the conversion increases as the time growing the bubble can become large compared to the rise time within the bubble. The decrease is most significant when increasing from 5 sccm to 10 sccm.

In a continuous run of 30 h in KCl and in $MnCl_2$(67)-KCl(33) methane conversion increases initially then stabilizes, Fig. 3. For $MnCl_2$(67)-KCl(33), at 1050 °C in the 12.5-cm molten salt bubble column, the conversion increased from 45% to almost 55% and stabilized. Similar behavior was observed for pure KCl, except that the steady state was reached after 5 h and the activity more than doubled, while still remaining well below that of the mixture $MnCl_2$(67)-KCl(33).

In pure KCl the carbon produced in the KCl melt intermixes with the salt forming a slurry. The increase of conversion in the first 5 h is likely due to the accumulation of suspended carbon in the melt resulting in an
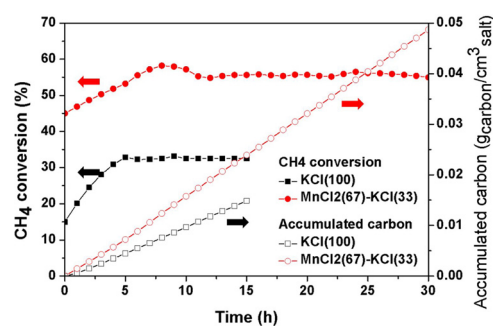

Fig. 3. CH_4 conversion over 30 h of continuous running for the 12.5-cm molten $MnCl_2$(67)-KCl(33) and KCl(100) bubble columns at 1050 °C: reactant gas = 5 sccm (100 mol% of CH_4), sweep gas = 50 sccm (100 mol% of Ar).

increased viscosity and slower bubble rise velocity (longer residence time). The measured bubble size doesn't change significantly over time. In KCl after 15 h the slurry is so viscose the bubble column can no longer be operated.

In the KCl-$MnCl_2$ mixtures there is increasing carbon suspended in the melt which might also increase the bubble residence time, however, there is greater separation of the carbon. The densities of $MnCl_2$-KCl mixtures (at the melting temperature) having a $MnCl_2$ molar fraction of less than 0.5 are lower than the density of carbon (1.9 g cm^{-3}) [34] and the carbon produced by pyrolysis sinks to the bottom of the melt. The densities of mixtures whose $MnCl_2$ molar fraction is higher than 0.5, are greater than carbon density, and the carbon formed by reaction floats on the surface of the molten $MnCl_2$-KCl (refer to S1 in Supplementary Data). Therefore, when the melt contains $MnCl_2$, the carbon can be removed, either at the top, or at the bottom of the column. This is important since the value of the process depends on the possibility of separating continuously the carbon produced by reaction.

Given the relatively high activity of the $MnCl_2$-KCl salt, we estimated the reactor length to achieve greater than 90% conversion at 950 °C and 1 atm of pressure to be only 450 cm (refer to S2 in Supplementary Data).

3.2. Separation and processing of the solid carbon product

The economics of methane pyrolysis in comparison to steam methane reforming depends on the ability to remove and sell or dispose of the solid carbon produced [43,44]. Economically, it is too expensive to lose the $MnCl_2$ if the carbon contains more than approximately 0.001 wt% $MnCl_2$. This amount of contamination would be tolerable in several commercial applications. However, if pyrolysis based hydrogen production were to replace SMR, and if the use of hydrogen for combustion fuel or fuel cells increases substantially, the amount of carbon co-product will be larger than any foreseeable carbon market. Unless new massive volume uses are found, the carbon needs to be safely disposed of. One potentially earth-compatible location would be in abandoned coal mines. In all cases it is best if the process could be run so that the carbon is not contaminated with the salt.

Both $MnCl_2$ and KCl are soluble in water and the salt contamination of the carbon was determined after washing the solid product 10 times with hot water (80 °C). Figs S4 and S5 in the Supplementary Data show electron micrographs and elemental mapping from energy dispersive X-ray spectroscopy (EDX) of the carbon which show homogeneous dispersions of Mn, K, and Cl in the carbon. The results for the elemental composition of the carbon from EDX and X-ray fluorescence (XRF) are shown in Table 2. There are two possibilities for charge imbalance in Table 2: 1. Manganese oxide or hydroxide was formed during cooling or washing, and we cannot detect the oxygen and hydrogen so it appears that we have uncompensated charge. 2. Borate ion is present from the boric acid which was added to be pelletized for XRF and we do not detect the protons, which again means that it seems that the charge in not balanced.

3.3. Characterization of carbon structure

A sheet-like carbon morphology was observed by electron microscopy in the water-washed solid products from the molten $MnCl_2$(67)-KCl(33), whereas the solid product from the molten KCl (100) has a more irregular shape Fig. 4. EDX confirmed that the observed structures were carbon and not impurities, Table 3. Although there are less gross morphological differences between the transmission electron microscopy (TEM) images of carbon from the $MnCl_2$(67)-KCl (33) and the carbon from KCl(100), Fig. 5, the electron diffraction pattern of the carbon shows clear difference in crystallinity. Multiple diffraction rings of carbon from the molten $MnCl_2$(67)-KCl(33) suggests a polycrystalline structure (Fig. 5b inset), while the delocalized diffraction ring of carbon from the molten KCl(100) implies an amorphous structure (Fig. 5f inset). Using high-resolution transmission electron microscopy (HRTEM), it was confirmed that more than 30 layers of graphene are stacked in the carbon from the molten $MnCl_2$(67)-KCl(33) (Fig. 5c and d). The approximate size of the crystalline grains measured with HRTEM (Fig. 5c), 11 nm, is consistent with the 11.6 nm value calculated using the Scherrer equation applied to the strong graphite-related XRD peak near 26.7° (Fig. 6a). In contrast, less than 10 layers of graphene are stacked in carbon from the molten KCl(100), Fig. 5g and h.

The XRD data from the carbon obtained from CH_4 pyrolysis in the molten $MnCl_2$(67)-KCl(33) shows the minor $MnCl_2$ and KCl peaks. The sharp graphite peak suggests that large crystalline C grains are produced, Fig. 6a. The absence of metallic manganese, manganese oxide, and manganese carbide peaks supports that the activity observed is from the molten salt and not from metallic compounds. The sharp KCl peak is observed in the diffraction data from the carbon obtained from the molten KCl(100); the solid carbon was completely intermixed with the molten salt and the solidified salt after cooling could not be fully separated by the water wash. The broad graphite peak implies the presence of relatively small crystalline grains of carbon. The SiO_2 peaks in both solid products from the molten KCl(100) and $MnCl_2$(67)-KCl (33) are attributed to the fracture of the quartz reactor during the cooling process.

Raman spectra of the carbon produced in the molten $MnCl_2$(67)-KCl (33) and KCl(100) were obtained to further characterize the carbon (Fig. 6b). The two major bands, commonly named the D and the G band, are observed. The ratio of the peak intensities I(G)/I(D) indicates the degree of graphitization since because the D band at 1350 cm^{-1} is attributed to the defects of the crystalline carbon, whereas the G band, at around 1585 cm^{-1}, is assigned to the sp^2 carbon networks [45]. The I (D)/I(G) ratio of the carbon from the molten $MnCl_2$(67)-KCl(33) is low ($\tilde{}$ 0.60), suggesting the highly graphitic structure of the produced carbon. The I(D)/I(G) ratio of KCl(100) is 1.37, which implies that the carbon is amorphous.

From the results of TEM, XRD, and Raman spectra, it can be concluded that the molten $MnCl_2$(67)-KCl(33) accelerated the production of more graphitic carbon through catalytic CH_4 pyrolysis, whereas, more amorphous carbon was generated by non-catalytic pyrolysis in molten KCl(100).

3.4. Mechanism of CH_4 pyrolysis in molten $MnCl_2$(67)-KCl(33) compared to KCl(100)

The relatively low apparent activation energy with a small pre-exponential factor for the pseudo-first order reaction rate constant and the production of highly graphitic carbon of the Mn containing salt is consistent with, but does not prove, that the reaction pathway on Mn-based is different than the assumed purely gas phase reaction in KCl. Furthermore, the product selectivities for CH_4 pyrolysis on molten $MnCl_2$(67)-KCl(33) and KCl(100) at 1050 °C and the same conversions are significantly different, Fig. 7. The CH_4 conversion was maintained at 30% for both the molten $MnCl_2$(67)-KCl(33) and KCl(100) by adjusting the position (depth) of the gas inlet tube to vary the residence time. An H_2 selectivity of 99% H_2 is observed in the molten $MnCl_2$(67)-KCl(33), whereas the molten KCl(100) shows less than 90% H_2
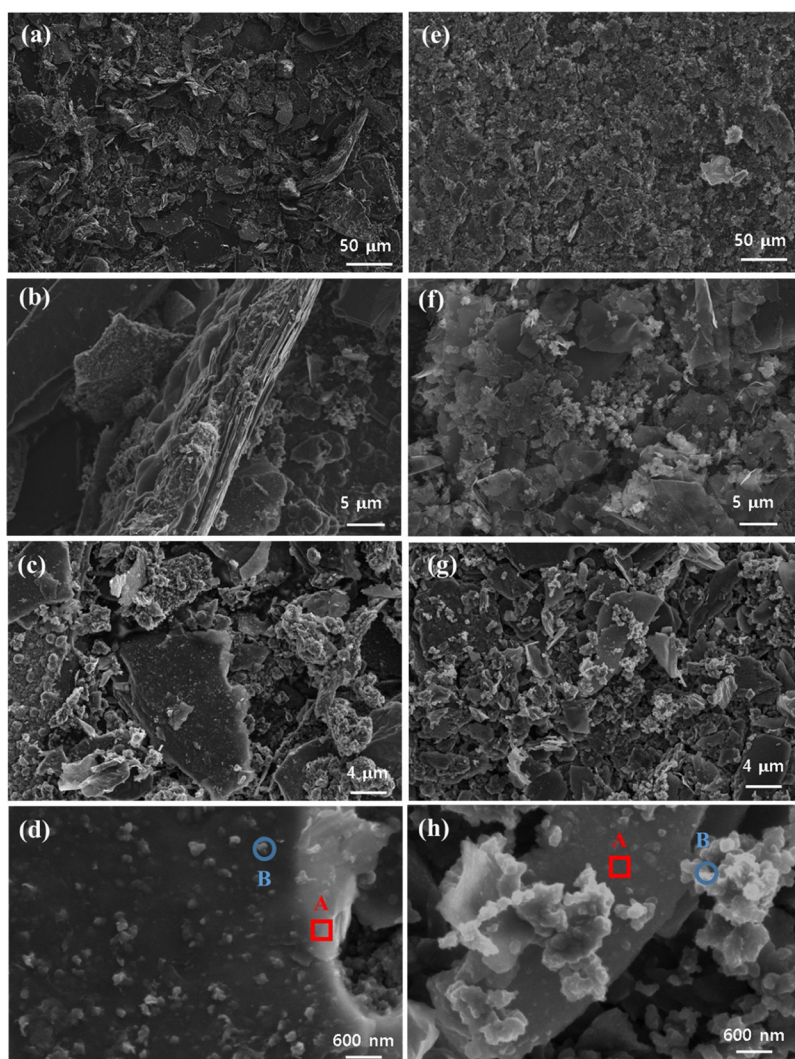
Table 2
Average compositions of the carbon after 10 times washing solid product from the molten $MnCl_2$(67)-KCl(33) and KCl(100).

Reaction melt	$MnCl_2$(67)-KCl(33)		KCl(100)	
Method	EDX	XRF	EDX	XRF
C (at.%)	96.22 ± 0.76	93.15 ± 0.82	91.97 ± 2.41	92.39 ± 1.03
K (at.%)	0.53 ± 0.09	1.56 ± 0.14	4.37 ± 0.99	4.23 ± 0.14
Mn (at.%)	0.99 ± 0.26	2.04 ± 0.23	N.A.	N.A.
Cl (at.%)	2.26 ± 0.33	3.25 ± 0.44	3.66 ± 0.69	3.38 ± 0.11

Fig. 4. SEM images of carbon extracted from MnCl$_2$(67)-KCl(33) (a–d) and KCl(100) (e–h) reaction mixtures at different magnifications and locations. EDX spot analysis was conducted on areas A and B (Table 3).

Table 3
EDX spot analysis of carbon from the molten MnCl$_2$(67)-KCl(33) and KCl(100) shown in Fig. 4.

Reaction melt	MnCl$_2$(67)-KCl(33)		KCl(100)	
Spot	A	B	A	B
C (at.%)	96.44 ± 0.24	96.00 ± 1.17	92.06 ± 3.63	91.83 ± 1.63
K (at.%)	0.48 ± 0.02	0.58 ± 0.11	4.33 ± 1.48	4.44 ± 0.74
Mn (at.%)	0.94 ± 0.05	1.04 ± 0.40	N.A.	N.A.
Cl (at.%)	2.14 ± 0.18	2.38 ± 0.44	3.61 ± 1.02	3.73 ± 0.54

selectivity with 10% selectivity to C$_{2+}$ hydrocarbons.

The rates of exchange for hydrogen with deuterium in mixtures of D$_2$ and CH$_4$ were measured in molten MnCl$_2$(67)-KCl(33) and KCl(100) at 900 °C. The mole ratio of D$_2$ and CH$_4$ was 5 with a total flowrate of 18 sccm. Deuterated products in the gas phase effluent stream was analyzed by mass spectroscopy. Fig. S6 shows that CH$_2$D$_2$ was the most abundant deuterated product, followed by CH$_3$D, CHD$_3$, and CD$_4$ on molten MnCl$_2$(67)-KCl(33). In contrast, on molten KCl(100), the deuterated products were in identical proportion to those observed for the sequential dehydrogenation in the gas phase reaction CH$_3$D (CH$_3$D > CH$_2$D$_2$ > CHD$_3$ > CD$_4$) [46].

Taken together, the different selectivities for intermediate hydrocarbons, different distribution of deuterated methanes in H-D exchange,

and the different carbon types from pyrolysis, support a different pyrolysis mechanism on MnCl$_2$(67)-KCl(33) and KCl(100). In the gas phase, pyrolysis is initiated with CH$_3$ radical generation. C$_{2+}$ hydrocarbons are produced from reactions of the CH$_3$ radicals [6,7]. The selectivity of C$_{2+}$ hydrocarbons and the composition of deuterated methane in molten KCl(100) are similar to what would be observed in a pure gas phase reaction. On the other hand, the absence of any significant C$_{2+}$ intermediate products and the presence of CH$_2$D$_2$ as the predominate exchange product observed from pyrolysis in molten MnCl$_2$(67)-KCl(33), imply a mechanism favoring further dehydrogenation associated with the MnCl$_2$ salt or very rapid reaction of the C$_{2+}$ intermediates on the catalytic surface as occurs on transition metals.

4. Conclusions

Mixtures of molten MnCl$_2$-KCl salts were investigated as a catalyst for CH$_4$ pyrolysis in a bubble column. The apparent activation energies decreased with increasing MnCl$_2$ concentration up to approximately 50 mol%. There seems to be a correlation between the catalytic activity and the concentration of tetrahedral MnCl$_4$$^{2-}$ ion to octahedral MnCl$_6$$^{4-}$, which implies that the tetrahedral MnCl$_4$$^{2-}$ is a potential catalytic ion in the melt. The remarkable synergy between KCl (a poor catalyst) and MnCl$_2$ (a mediocre catalyst) to provide a good catalyst may be related
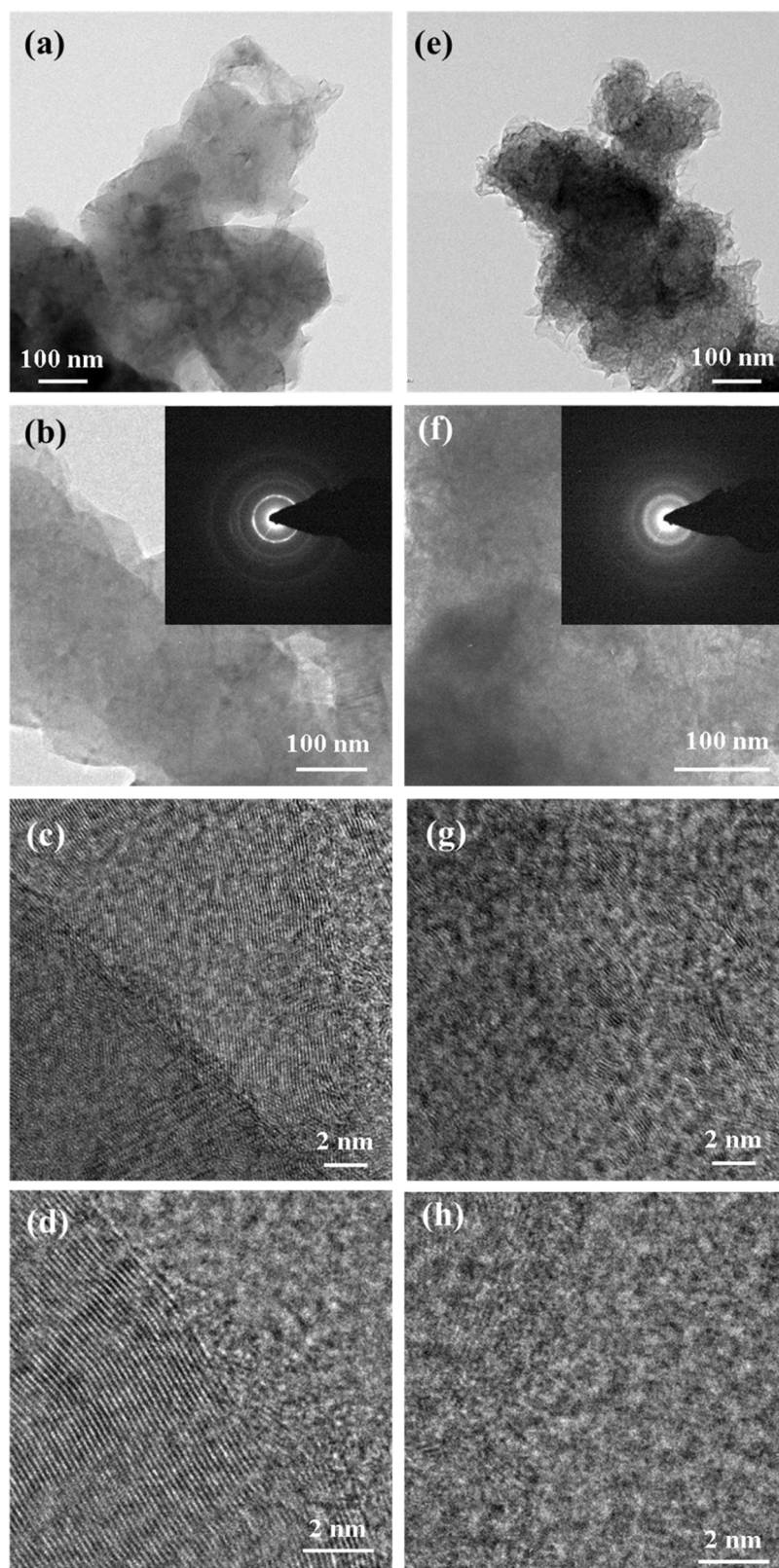
Fig. 5. TEM images of carbon extracted from $MnCl_2$(67)-KCl(33) (a and b) and KCl(100) (e and f) with the insets showing the diffraction rings. HRTEM images of carbon extracted from $MnCl_2$(67)-KCl(33) (c and d) and KCl(100) (g and h).

to the presence of these complex ions.

The pre-exponential factor of the rate constant in molten $MnCl_2$-KCl mixtures also decreases with increasing $MnCl_2$ up to 50 mol%, possibly suggesting that the pyrolysis pathway within the gas bubble changes from a predominately gas phase uncatalyzed reaction in the KCl melt to a reaction catalyzed by the melt surface or vapor due to the presence of $MnCl_2$. Considering overall compensation in the observed rates between decreasing activation energy and increasing pre-exponential factor, the
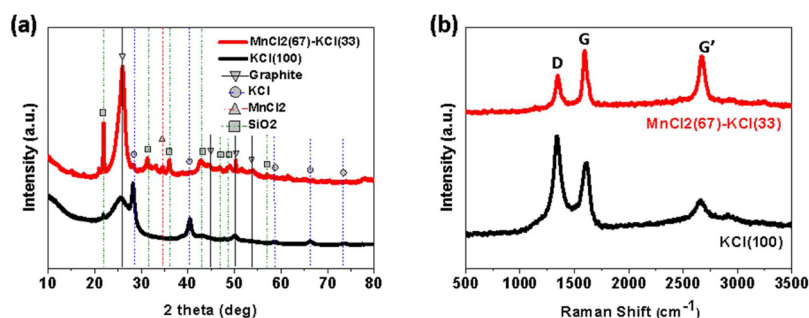
Fig. 6. (a) XRD patterns and (b) Raman spectra of carbon from $MnCl_2(67)$-KCl(33) and KCl(100) reaction mixtures.
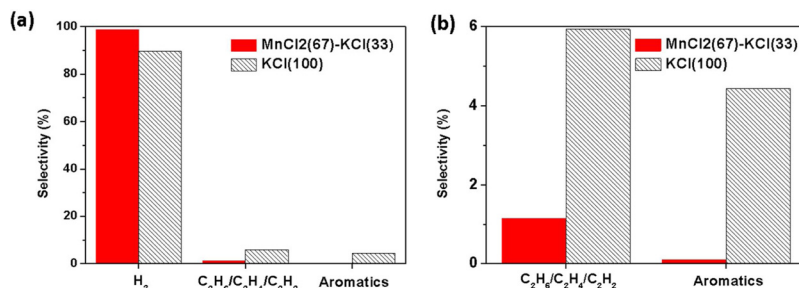

Fig. 7. (a) H_2 and (b) C_{2+} hydrocarbon selectivities of the CH_4 pyrolysis in the molten $MnCl_2(67)$-KCl(33) and KCl(100) at 1050 °C: reactant gas = 10 sccm (100 mol % of CH_4), sweep gas = 50 sccm (100 mol% of Ar) (CH_4 conversion was 30% in both cases).

methane conversion in the molten $MnCl_2$-KCl mixture was highest in a mixture of 67:33.

The melt activity is stable for at least 30 h, producing a separable solid carbon product due to the relatively high density of $MnCl_2$-KCl melt and low wettability of the carbon product by a melt. The carbon produced was graphitic and the salt contamination can be reduced to less than 7 at% with water washing.

The 99% H_2 selectivity when using molten $MnCl_2$-KCl suggests C_{2+} hydrocarbons are either not formed or are rapidly decomposed on the surface. In contrast 10% selectivity to C_{2+} hydrocarbons was observed in pure KCl melt at the same CH_4 conversion, 30%. The relatively large amount of further deuterated methane, CH_2D_2, in H-D exchange on molten $MnCl_2$-KCl signifies that the reaction pathway is different than the assumed purely gas phase reaction in pure KCl melt, where CH_3D is the most abundant deuterated methane.

Considering the high CH_4 conversion, H_2 selectivity, and deuterated methane species seen using $MnCl_2$-KCl melt, it can be surmised that the CH_4 pyrolysis is accelerated and the graphitic carbon is generated on the surface of the molten $MnCl_2$-KCl. A single bubble model is in reasonable agreement with the experimental data within the molten salt bubble column at lab scales.

Acknowledgements

Appendix A. Supplementary data

Supplementary material related to this article can be found, in the online version, at doi:https://doi.org/10.1016/j.apcatb.2019.05.026.

References

[1] A. Midilli, M. Ay, I. Dincer, M.A. Rosen, On hydrogen and hydrogen energy strategies I: current status and needs, Renew. Sust. Energy Rev. 9 (2005) 255–271.

[2] A. Midilli, M. Ay, I. Dincer, M.A. Rosen, On hydrogen and hydrogen energy strategies II: future projections affecting global stability and unrest renew, Sust. Energy Rev. 9 (2005) 273–287.

[3] N.Z. Muradov, T.N. Veziroglu, Green" path from fossil-based to hydrogen economy: an overview of carbon-neutral technologies, Int. J. Hydrogen Energy 33 (2008) 6804–6839.

[4] J. Conti, P. Holtberg, J. Diefenderfer, A. LaRose, J.T. Turnure, L. Westfall, International Energy Outlook 2016 With Projections to 2040, ; USDOE Energy Information Administration (EIA), Office of Energy Analysis, Washington, DC (United States), 2016 pp. Medium: ED; Size: 290 p.

[5] F. Billaud, C. Gueret, J. Weill, Thermal-decomposition of pure methane at 1263-K - experiments and mechanistic modeling, Thermochim. Acta 211 (1992) 303–322.

[6] C.J. Chen, M.H. Back, R.A. Back, The thermal decomposition of methane. II. Secondary reactions, autocatalysis and carbon formation; non-arrhenius behaviour in the reaction of CH_3 with ethane, Can. J. Chem. 54 (1976) 3175–3184.

[7] C.J. Chen, M.H. Back, R.A. Back, The thermal decomposition of methane. I. Kinetics of the primary decompositionto C_2H_6 + H_2; Rate Constant for the homogeneous unimolecular dissociation of methane and its pressure dependence, Can. J. Chem. 53 (1975) 3580–3590.

[8] A. Holmen, O. Olsvik, O.A. Rokstad, Pyrolysis of natural-gas - chemistry and process concepts, Fuel Process. Technol. 249-267.

[9] M. Pudukudy, Z. Yaakob, M.Z. Mazuki, M.S. Takriff, S.S. Jahaya, One-pot sol-gel synthesis of MgO nanoparticles supported nickel and iron catalysts for undiluted methane decomposition into CO_x free hydrogen and nanocarbon, Appl. Catal. B: Environ. 218 (2017) 298–316.

[10] L. Zhou, L.R. Enakonda, M. Harb, Y. Saih, A. Aguilar-Tapia, S. Ould-Chikh, J.-l. Hazemann, J. Li, N. Wei, D. Gary, P. Del-Gallo, J.-M. Basset, Fe catalysts for methane decomposition to produce hydrogen and carbon nano materials, Appl. Catal. B: Environ. 208 (2017) 44–59.

[11] A. Rastegarpanah, M. Rezaei, F. Meshkani, H. Dai, H. Arandiyan, Thermocatalytic decomposition of methane over mesoporous $Ni/xMgO·Al_2O_3$ nanocatalysts, Int. J. Hydrogen Energy 43 (2018) 15112–15123.

[12] A. Rastegarpanah, M. Rezaei, F. Meshkani, K. Zhang, X. Zhao, W. Pei, Y. Liu, J. Deng, H. Arandiyan, H. Dai, Influence of group VIB metals on activity of the Ni/MgO catalysts for methane decomposition, Appl. Catal. B: Environ. 248 (2019) 515–525.

[13] K. Otsuka, S. Takenaka, H. Ohtsuki, Production of pure hydrogen by cyclic decomposition of methane and oxidative elimination of carbon nanofibers on

supported-Ni-based catalysts, Appl. Catal. A. Gen. 273 (2004) 113–124.

[14] V.R. Choudhary, S. Banerjee, A.M. Rajput, Continuous production of H_2 at Low temperature from methane decomposition over Ni-containing catalyst followed by gasification by steam of the carbon on the catalyst in Two parallel reactors operated in cyclic manner, J. Catal. 198 (2001) 136–141.

[15] D. Kang, J.W. Lee, Enhanced methane decomposition over nickel-carbon-B_2O_3 core-shell catalysts derived from carbon dioxide, Appl. Catal. B: Environ. 186 (2016) 41–55.

[16] A. Eatemadi, H. Daraee, H. Karimkhanloo, M. Kouhi, N. Zarghami, A. Akbarzadeh, M. Abasi, Y. Hanifehpour, S.W. Joo, Carbon nanotubes: properties, synthesis, purification, and medical applications, Nanoscale Res. Lett. 9 (2014) 393–408.

[17] T. Geissler, M. Plevan, A. Abanades, A. Heinzel, K. Mehravaran, R.K. Rathnam, C. Rubbia, D. Salmieri, L. Stoppel, S. Stuckrad, A. Weisenburger, H. Wenninger, T. Wetzel, Experimental investigation and thermo-chemical modeling of methane pyrolysis in a liquid metal bubble column reactor with a packed bed, Int. J. Hydrogen Energy 40 (2015) 14134–14146.

[18] M. Plevan, T. Geissler, A. Abanades, K. Mehravaran, R.K. Rathnam, C. Rubbia, D. Salmieri, L. Stoppel, S. Stuckrad, T. Wetzel, Thermal cracking of methane in a liquid metal bubble column reactor: experiments and kinetic analysis, Int. J. Hydrogen Energy 40 (2015) 8020–8033.

[19] I. Schultz, D.W. Agar, Decarbonisation of fossil energy via methane pyrolysis using two reactor concepts: fluid wall flow reactor and molten metal capillary reactor, Int. J. Hydrogen Energy 40 (2015) 11422–11427.

[20] A. Abanades, R.K. Rathnam, T. Geissler, A. Heinzel, K. Mehravaran, G. Muller, M. Plevan, C. Rubbia, D. Salmieri, L. Stoppel, S. Stuckrad, A. Weisenburger, H. Wenninger, T. Wetzel, Development of methane decarbonisation based on liquid metal technology for CO_2-free production of hydrogen, Int. J. Hydrogen Energy 41 (2016) 8159–8167.

[21] T. Geissler, A. Abanades, A. Heinzel, K. Mehravaran, G. Muller, R.K. Rathnam, C. Rubbia, D. Salmieri, L. Stoppel, S. Stuckrad, A. Weisenburger, H. Wenninger, T. Wetzel, Hydrogen production via methane pyrolysis in a liquid metal bubble column reactor with a packed bed, Chem. Eng. J. 299 (2016) 192–200.

[22] A.V. Gulevich, P.N. Martynov, V.A. Gulevsky, V.V. Ulyanov, Technologies for hydrogen production based on direct contact of gaseous hydrocarbons and evaporated water with molten Pb or Pb-Bi, Energy Convers. Manage. 49 (2008) 1946–1950.

[23] D.C. Upham, V. Agarwal, A. Khechfe, Z.R. Snodgrass, M.J. Gordon, H. Metiu, E.W. McFarland, Catalytic molten metals for the direct conversion of methane to hydrogen and separable carbon, Science 358 (2017) 917–920.

[24] M. Steinberg, Fossil fuel decarbonization technology for mitigating global warming, Int. J. Hydrogen Energy 24 (1999) 771–777.

[25] C.N. Kenney, Molten-Salt catalysis of gas reactions, Catal. Rev. Sci. Eng. 11 (1975) 197–224.

[26] E. Sada, H. Kumazawa, M. Kudsy, Pyrolysis of lignins in molten-Salt media, Ind. Eng. Chem. Res. 31 (1992) 612–616.

[27] R. Adinberg, M. Epstein, J. Karni, Solar gasification of biomass: a molten salt pyrolysis study, J. Sol. Energy. Eng. 126 (2004) 850–857.

[28] X.F. Liu, M. Antonietti, Molten salt activation for synthesis of porous carbon nanostructures and carbon sheets, Carbon 69 (2014) 460–466.

[29] X.F. Liu, C. Giordano, M. Antonietti, A facile molten-Salt route to graphene synthesis, Small 10 (2014) 193–200.

[30] W.P. Liu, L. Ackermann, Manganese-catalyzed C-H activation, Acs Catal. 6 (2016) 3743–3752.

[31] H.J. Seifert, J. Uebach, Thermodynamic and structural investigations of chlorides in the systems $KCl/MgCl_2$ and $KCl/MnCl_2$, J. Solid State Chem. 59 (1985) 86–94.

[32] A.S. Kucharski, S.N. Flengas, Electrical conductivities and molar volumes in binary-systems $MnCl_2$-LiCl, $MnCl_2$-NaCl, $MnCl_2$-KCl, $MnCl_2$-RbCl, $MnCl_2$-CsCl, J. Electrochem. Soc. 121 (1974) 1298–1308.

[33] T. Kei, N. Tetsuro, Raman spectra of the molten $MnCl_2$–KCl SYSTEM, Chem Lett. 4 (1975) 351–356.

[34] T. Kei, T. Yoshiki, N. Tetsurō, Density and refractive index of the molten $MnCl_2$-KCl system, Jpn. J. Appl. Phys. 15 (1976) 1637.

[35] H. Ohno, K. Furukawa, K. Tanemoto, Y. Tagaki, T. Nakamura, Structural analysis of some molten materials by X-ray diffraction. Part 3.—$MnCl_2$, J. Chem. Soc. 74 (1978) 804–808 Faraday 1.

[36] T. Kei, N. Tetsurō, ESR spectra of the molten $MnCl_2$–KCl system, Jpn. J. Appl. Phys. 17 (1978) 1561–1564.

[37] S. Tadashi, I. Mitsuru, S. Toshiyuki, Mass-spectrometric measurements of thermo-dynamic properties of the molten KCl–$MnCl_2$ system, Bull. Chem. Soc. Jpn. 56 (1983) 2415–2419.

[38] L. Stoppel, T. Fehling, T. Geissler, E. Baake, T. Wetzel, Carbon dioxide free production of hydrogen, Final Limtech Colloquium and International Symposium on Liquid Metal Technologies 228 (2017).

[39] T. Keipi, K.E.S. Tolvanen, H. Tolvanen, J. Konttinen, thermo-catalytic decomposition of methane: the effect of reaction parameters on process design and the utilization possibilities of the produced carbon, Energ Convers Manage 126 (2016) 923–934.

[40] H.B. Palmer, T.J. Hirt, The activation energy for the pyrolysis of methane[1], J. Phys.Chem. 67 (1963) 709–711.

[41] E.R. Gilliland, P. Harriott, Reactivity of deposited carbon, Ind. Eng. Chem. Res. 46 (1954) 2195–2202.

[42] N. Muradov, F. Smith, A. T-Raissi, Catalytic activity of carbons for methane decomposition reaction, Catal. Today 102–103 (2005) 225–233.

[43] X. Zhang, A. Kätelhön, G. Sorda, M. Helmin, M. Rose, A. Bardow, R. Madlener, R. Palkovits, A. Mitsos, CO_2 mitigation costs of catalytic methane decomposition, Energy 151 (2018) 826–838.

[44] B. Parkinson, P. Balcombe, J.F. Speirs, A.D. Hawkes, K. Hellgardt, Levelized cost of CO_2 mitigation from hydrogen production routes, Energy Environ. Sci. (2019).

[45] M.A. Pimenta, G. Dresselhaus, M.S. Dresselhaus, L.G. Cancado, A. Jorio, R. Saito, Studying disorder in graphite-based systems by raman spectroscopy, Phys. Chem. Chem. Phys. 9 (2007) 1276–1291.

[46] G. Pratt, D. Rogers, Homogeneous isotope Exchange-reactions .2. CH_4-D_2, J. Chem. Soc. 72 (1976) 2769–2776 Faraday 1.